Palaeogeography, Palaeoclimatology, Palaeoecology 568 (2021) 110289

Contents lists available at ScienceDirect

Palaeogeography, Palaeoclimatology, Palaeoecology

journal homepage: www.elsevier.com/locate/palaeo

Invited Research Article

Increased frequency of extreme precipitation events in the North Atlantic during the PETM: Observations and theory

William D. Rush [a,*], Jeffrey T. Kiehl [a], Christine A. Shields [b], James C. Zachos [a]

[a] University of California, Santa Cruz, 1156 High Street, Santa Cruz, CA 95064, USA
[b] National Center for Atmospheric Research, PO Box 3000, Boulder, CO 80307, USA

ARTICLE INFO

Keywords:
Paleocene-Eocene thermal maximum
Model-data comparison
Climate model
Mid-Atlantic
Pyrenees

ABSTRACT

Climate model simulations of the PETM (Paleocene-Eocene Thermal Maximum) warming have mainly focused on replicating the global thermal response through greenhouse forcing, i.e. CO_2, at levels compatible with observations. Comparatively less effort has gone into assessing the skill of models to replicate the response of the hydrologic cycle to the warming, particularly on regional scales. Here we have assembled proxy records of regional precipitation, focusing on the Mid-Atlantic Coasts of North America (New Jersey) and Europe (Spain) to test the response of the hydrologic system to greenhouse gas forcing of the magnitude estimated for the PETM (i.e., 2×). Given evidence that the PETM initiated during a maximum in eccentricity, this includes the response under neutral and extreme orbital configurations. Modeled results show excellent agreement with observations in Northern Spain, with a significant increase in both mean annual and extreme precipitation resulting from increased CO_2 levels under a neutral orbit. The Mid Atlantic Coast simulations agree with observations showing increases in both overall and extreme precipitation as a result of CO_2 increases. In particular, the development of sustained atmospheric rivers might be significantly contributing to the extremes of the eastern Atlantic, whereas extratropical cyclones are likely contributing to the extremes in the western Atlantic. With an eccentric orbit that maximizes insolation during boreal summer, there is a suppression of extreme precipitation events in the eastern Atlantic and an amplification in the western Atlantic, which may account for observations in the relative timing of the sedimentary response to the carbon isotope excursion associated with the PETM.

1. Introduction

In response to greenhouse warming, the hydrological cycle is anticipated to intensify, as higher temperatures lead to a higher saturation vapor pressure, thus increasing the holding capacity of the atmosphere (Held and Soden 2006). On a global scale the changes in evaporation will be manifested in large part by increased transport of vapor from the subtropics poleward. However, there is a good deal of variability between models (Carmichael et al. 2018) and within models both spatially and in how this intensification may manifest itself. Therefore, simple estimates of mean annual precipitation will not adequately capture the climatic response (Pfahl et al. 2017). This is due to the fact that climates are not influenced solely by the amount of precipitation that falls, but rather how it falls, e.g. whether the precipitation is evenly distributed throughout the year or is highly seasonal or episodic (e.g., cyclones, atmospheric rivers). This is particularly relevant to forecasting changes in the frequency and intensity of droughts and thus the impacts of global warming on terrestrial ecosystems and agriculture.

While models can provide excellent approximations of past or future climate states, there are inherent limitations due to the tradeoff between model complexity and computational requirements. Processes that occur at scales smaller than the resolution of the model must be parameterized, e.g. cloud physics, and there is disagreement on the dynamics of these processes and how they are managed (Arakawa 2004; Jakob 2010; McFarlane 2011; Christensen 2020). As a consequence, the inability of models to simulate dynamics on finer spatial and temporal scales becomes increasingly problematic as the forcing (i.e., GHG) deviates further from the modern state. This is particularly so with the simulation of processes such as cyclones and atmospheric rivers that can influence the tail end distribution of precipitation extremes.

One potential strategy for assessing theory on intensification of the hydrologic cycle is to turn to Earth's past episodes of extreme greenhouse warming as represented in geologic archives (Carmichael et al. 2018). The Eocene epoch in particular is characterized by a series of

* Corresponding author.
E-mail addresses: wrush@ucsc.edu (W.D. Rush), jkiehl@ucsc.edu (J.T. Kiehl), shields@ucar.edu (C.A. Shields), jzachos@ucsc.edu (J.C. Zachos).

https://doi.org/10.1016/j.palaeo.2021.110289
Received 29 October 2020; Received in revised form 28 January 2021; Accepted 5 February 2021
Available online 11 February 2021

rapid warming events referred to as "hyperthermals" (e.g., Littler et al. 2014). Each of these was likely driven by release of isotopically depleted C and rising greenhouse gas levels as evidenced by carbon isotope excursions and deep-sea carbon dissolution (i.e., ocean acidification). The largest carbon release occurred during the Paleocene-Eocene Thermal Maximum, or PETM, with estimates ranging from less than 4500 GtC to over 10,000 GtC (Zeebe et al. 2009; Gutjahr et al. 2017). As a consequence, mean global temperature rose over 5 °C dramatically impacting regional climate and ecosystems (McInerney and Wing 2011). While the exact mechanism that triggered the carbon release has been disputed, it has been suggested that the PETM is the closest approximation to current anthropogenic global warming, although at a slower rate (Zeebe and Zachos 2013).

The response of the global hydrologic cycle to the PETM warming was significant. Evidence for a mode shift in precipitation patterns or an "intensification" exists in locations around the world (Carmichael et al. 2018). On a global scale the planet appeared to become "wetter" consistent with an increase in the atmospheric holding capacity and transport of vapor with higher temperature. In detail, however, the mode of intensification varied regionally, with some regions appearing to become wetter, other regions dryer, or both in the sense of a change in the cycle of precipitation on seasonal or longer time scales. Some of the most notable changes have been observed in coastal P-E boundary sections located along the margins of the north Atlantic (John et al. 2008; Kopp et al. 2009; Schmitz and Pujalte 2007). For example, the western Atlantic margin, the North Sea, and Bay of Biscay experienced an influx of kaolinite (Gibson et al. 2000; Kemp et al. 2016; Schmitz et al. 2001). This increase in kaolinite has also been noted at a number of other locations including central China, Tanzania, and Antarctica (Chen et al. 2016; Handley et al. 2012; Robert and Kennett 1994). In most cases, it has been argued that this shift in clay mineral assemblage is not the result of enhanced chemical weathering further leaching the clays, but rather an enhanced physical weathering eroding out previously deposited sediment (Gibson et al. 2000; Handley et al. 2012; John et al. 2012).

Previous modeling and observational studies of the PETM have addressed intensification of the hydrologic cycle on a global scale (Carmichael et al. 2018; Kiehl et al. 2018). Here, we assess regional intensification, focusing on the margins of the North Atlantic where observations exist for both coasts and thus have the potential to provide insight into the response of both large and small-scale processes. This includes processes such as atmospheric rivers and extratropical cyclones which play a role in the frequency of extreme precipitation events along eastern ocean boundaries and western ocean boundaries respectively (Laing and Evans 2011; Ralph 2019). Further detail on the changes to tropical cyclones and atmospheric rivers can be found in Kiehl et al., in Review and Shields et al., 2021 respectively, which complement this study.

This study utilizes a 2 by 2 experimental design wherein the effects of CO_2 forcing and orbital forcing can be analyzed both independently and in conjunction in order to disentangle their effects. It has been argued

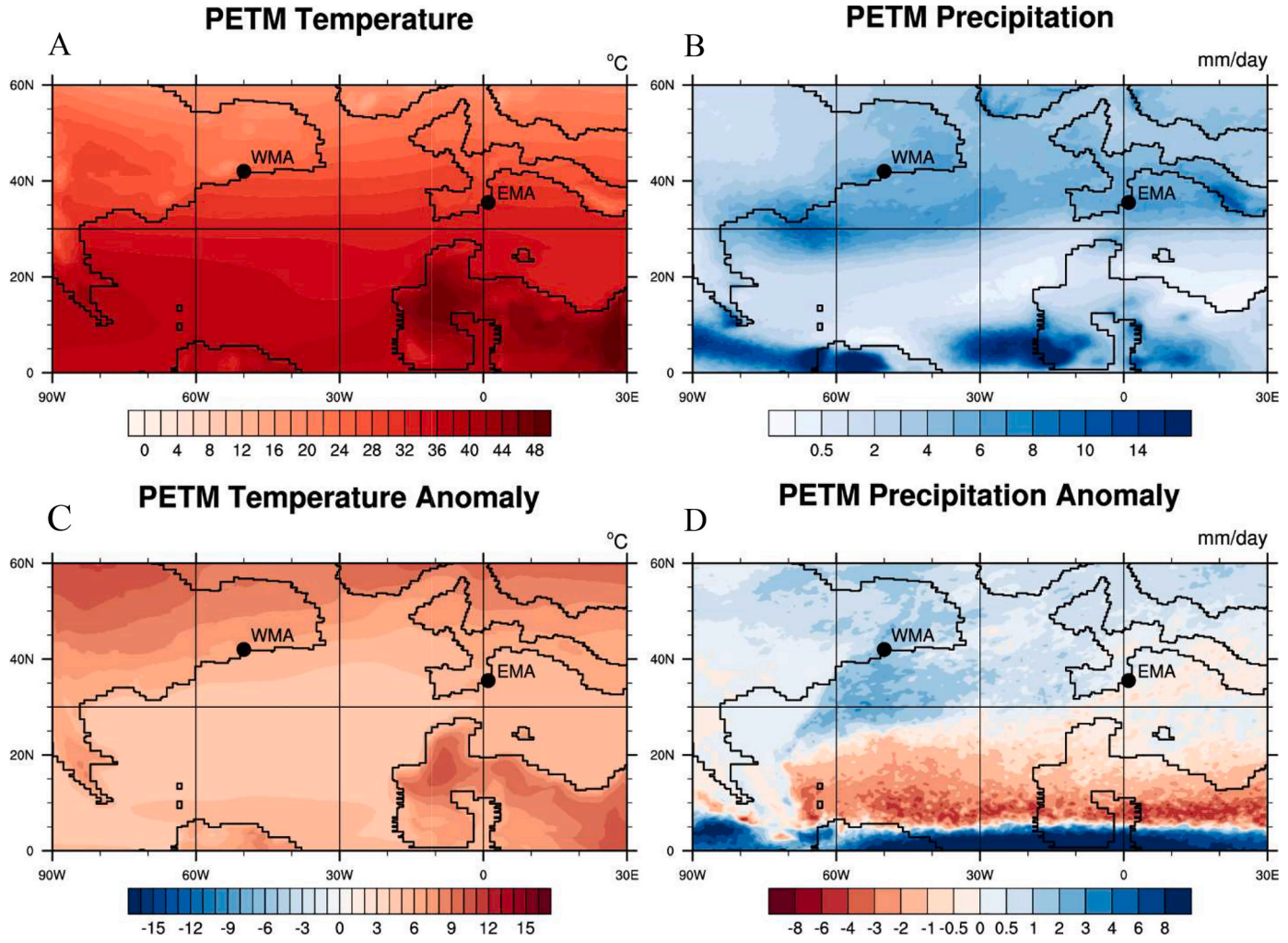

Fig. 1. Paleoreconstruction of the of the North Atlantic during PETM overlain with CAM5 simulated PETM (pCO_2 = 1590 ppmv) mean annual temperature (A), precipitation rate (B), and anomalies for each (C, D) relative to the late Paleocene (pCO_2 = 680 ppmv). Study locations marked by black dots. WMA = Western Mid Atlantic, EMA = Eastern Mid Atlantic.

that the onset of the PETM occurred near an eccentricity maximum (100 or 405-thousand-year; e.g., Zeebe and Lourens 2019) suggesting some combination of orbital and greenhouse forcing on climate. Given the potential influence of orbital configuration on seasonal precipitation patterns and intensity in the Northern Hemisphere (e.g., the monsoons), analyzed simulations include an orbital configuration that maximizes insolation for NH summers. To that end, we utilize the latest simulations of precipitation of the Community Atmosphere Model, Version 5.3, hereafter referred to as CAM5, as configured with late Paleocene and PETM boundary conditions, GHG forcing, and orbital configurations (Fig. 1). We then analyze modeled hydrologic changes against compiled records from the North Atlantic margin and the Basque Basin to determine if the modeled response adequately captures the signal preserved in the sediment record. In particular, we assess the relative fit of the simulations of precipitation on scales relevant to the reconciliation of observations on a regional scale. While the observational constraints are limited in terms of constraining the exact nature of changes in precipitation, either amounts or seasonal distribution, we are able to combine multiple qualitative estimates of precipitation change in order to assess model fit.

2. Materials and methods

2.1. Depositional constraints on Atlantic coastal hydrology

The observational constraints for the western Mid-Atlantic (hereafter referred to as WMA) region come mainly from sites along from the New Jersey coastal plain (Fig. 1, Fig. S1). The sediments obtained from these cores were deposited in the Salisbury Embayment on a shallow continental shelf on a passive margin. The full sedimentary succession ranges from the Cretaceous through the modern and is underlain by crystalline basement. The studied interval is comprised of the upper Paleocene Aquia Formation, a glauconitic, fine silty, clay-rich sandstone, overlain by lower Eocene Marlboro Clay, which is in turn overlain by the Nanjemoy formation, a glauconitic, fine, silty, clay-rich sandstone similar to the Aquia (Self-Trail et al. 2017). All records of sedimentation and climate from the New Jersey shelf sequences unequivocally support a significant mode shift in the regional hydrologic cycle during the PETM. Sedimentation rates increased several-fold despite rising sea level as the flux of siliciclastics, including kaolinite, to the coastal ocean increased (Gibson et al. 2000; John et al. 2008; Stassen et al. 2012). Moreover, dinoflagellate assemblages shifted from open marine toward more low-salinity tolerant species and bacterial magnetofossils akin to the distribution observed within modern-day sediments off the coast of the Amazon river increased in abundance and diversity (Sluijs and Brinkuis, 2009; Kopp et al. 2009; Lippert and Zachos 2007). Collectively, the changes in depositional rates, lithology, and fossil assemblages are consistent with increased runoff and erosion on a mean annual and/or seasonal basis. Similar observations have been reported for P-E sections approximately 75 miles to the southwest in Maryland (Lyons et al. 2019).

The primary observational constraints for the eastern Mid-Atlantic (hereafter referred to as EMA) considered in this study come from units deposited in the Basque Basin of Northern Spain. These basins contain PETM sections deposited in terrestrial and shallow and deep marine settings (Fig. 1, Fig. S1). The terrestrial sections are comprised of paleosols and floodplain deposits deposited in the late Paleocene that transition to the large-clast (up to 65 cm) Claret Conglomerate during the CIE before transitioning back to deposits similar to the late-Paleocene (Schmitz and Pujalte 2007). Computations of channel dimensions suggest a substantial rise in discharge rates during the PETM (increasing from $31 \pm 4.3\ m^3s^{-1}$ to $253 \pm 102\ m^3s^{-1}$) (Chen et al. 2018). The deep marine sections are comprised primarily of hemipelagic limestones and marlstones transitioning into low-calcareous kaolinite-rich clays and silty clays during the CIE, returning to hemipelagic limestones and marlstones after the recovery (Pujalte et al. 2015). During the peak PETM, sedimentation rates in the distal, deep-water portion of the basin are estimated to have increased 4-fold (Dunkley Jones et al. 2018). Although debated, several sites appear to show a "temporal lag" between the onset of the PETM and the changes in sedimentation (Duller et al. 2019).

2.2. PETM climate simulations

A series of experiments simulating the PETM warming have been conducted (Kiehl et al., in prep; Shields et al., in prep) utilizing the high resolution (0.25°) CAM5, Version 5.3, with fixed sea surface temperatures and finite volume dynamical (FV) core, with 30 levels in the vertical for the atmosphere component (Neale et al. 2010; Park et al. 2014). The land component is the Community Land Model, Version 4 (CLM4) (Lawrence et al. 2011), also at 0.25° resolution, with the river transport model (RTM) at 1° resolution. Organic aerosol emissions were produced by running MEGAN (Model of Emissions of Gases and Aerosols) approximated from PETM biomes using DeepMIP protocols (Guenther et al. 2012; Lunt et al. 2017). The boundary conditions and sea surface temperatures from this model were obtained from a fully coupled LP and PETM FV 2° CESM1.2.2 (Community Earth System Model, Version 1.2) with output taken at a monthly temporal resolution over 1800 years.

Output was obtained from CAM5 at 6 hourly, daily, and monthly temporal resolution for over 20 years. The model was run with late Paleocene CO_2 values of 680 ppmv (hereafter referred to as LP) and PETM CO_2 values of 1590 ppmv (hereafter referred to as PETM). Methane was held at 16 ppmv in all runs. Additionally, in order to test the impact of orbital forcing, the model was run with both a neutral orbit and a configuration that maximized solar insolation over the northern hemisphere (i.e. High eccentricity, perihelion NH summers), hereafter referred to as OrbMax. Solar forcing was calculated based on a solar constant of 1355 Wm^{-2} consistent with Kiehl et al. (2018). The four runs are therefore referred to as LP, PETM, LP OrbMax, PETM OrbMax (Table 1). Paleocoordinates for each location were set over a 2° by 2° area and were taken from the DeepMIP protocols (Lunt et al. 2017). EMA was set to 34.5°-36.5°N, 0°-2°E. WMA was set to 41°-43°N, 49°-51°W. In order to account for the time required for the model to reach equilibration, data was trimmed to the final 15 years of the 20-year model run.

The parameters of interest include median and 1st and 3rd quartile monthly precipitation and runoff to track both annual and seasonal variation, and exceedance frequency to track storm intensity and to track changes in frequency of storm events. Exceedance frequency is calculated as $\boldsymbol{P} = \boldsymbol{m} \div (\boldsymbol{n} + \mathbf{1})$, wherein $\boldsymbol{P}$ is the exceedance frequency, $\boldsymbol{m}$ is the rank of a given event, and $\boldsymbol{n}$ is the total number of events.

3. Results

PETM simulations show increases in temperatures with the largest increases occurring at high latitudes, and changes in mean annual precipitation consistent with the "wet gets wetter, dry gets drier" trend noted in Held and Soden (2006), with increases to precipitation occurring in the tropics and high latitudes and decreases in the subtropics (Fig. 1). Applying the OrbMax configuration results in enhanced seasonality of temperatures in the northern hemisphere, i.e. hotter summers and colder winters, with a more varied hydrologic response, demonstrating latitudinal shifts in precipitation patterns and changes in intensity of seasonal precipitation (Figs. S3-S10).

Precipitation data from the high-resolution 0.25° model (CAM5) for all simulations was extracted and evaluated for 2° by 2° regions in the

Table 1
Explanation of model parameter abbreviations.

	Neutral Orbit	Maximized NH Summers
Low CO_2 (680 ppmv)	LP	LP OrbMax
High CO_2 (1590 ppmv)	PETM	PETM OrbMax

Mid-Atlantic and Pyrenees. The extracted output includes annual precipitation and runoff, exceedance frequency of precipitation events and runoff, and median and quartile precipitation and runoff for each month.

For the WMA, mean annual precipitation increases by 14.3% from 1885 mm/year in the LP run to 2155 mm/year in the PETM run; however, this is highly seasonal, with the largest overall increases occurring during September through December when comparing the LP and PETM (Fig. 2). There is a significant increase in the exceedance frequency of individual storm events and runoff events, and intensity of individual storm events experiences its greatest change in May through October (Figs. 2, 3).

Applying the OrbMax configuration to the LP run results in mean annual precipitation increases of 7.3% from 1885 to 2024 mm/year. Average monthly total precipitation is higher for every month, but the greatest differences are in July and August, likely due to the higher insolation during summer months. In terms of the intensity of individual events, there is little change in the 3rd quartile between the LP and LP OrbMax configurations, but the exceedance frequency demonstrates dramatic increases to both runoff and precipitation rates (Figs. 2, 3).

For the PETM run, applying the OrbMax configuration resulted in changes to overall precipitation intermediate to those observed from either CO_2 or changing the orbital configuration alone, with an increase of 11.5% to 2101 mm/year compared to the LP run. The exceedance frequency showed an increase in storm intensity, with increases largely occurring in summer months, similar to CO_2 forcing alone (Figs. 2,3).

Modeled runoff for the WMA region shows similar trends to precipitation when comparing the model runs; however, there is a shift in the seasonal timing, perhaps due to seasonal variations in evapotranspiration owing to increased insolation and elevated temperatures in summer months or groundwater recharge within the land component of the model (Figs. 2, 3). The PETM run has the highest rate of runoff, with an average of 1311 mm/year, a 36.8% increase over the 958 mm/year during the LP run, with the average monthly totals increasing in every month except February and March, and the greatest increases occurring in October through January. In contrast to precipitation, the greatest variability also occurs in the winter months.

Hydrologic shifts in the EMA are even more pronounced, with an increase of 55.2% in mean annual precipitation from 1531 mm/year in the LP run to 2376 mm/year in the PETM run. On a monthly basis, the increase in precipitation is spread throughout the year, with the largest changes occurring in January, February, and March. Much of this increase appears to be in the form of more extreme precipitation during these months as evidenced by the shift in the 3rd quartile during this time (Figs. 2, 3).

However, unlike the WMA, relative to the neutral orbit LP at OrbMax resulted in a net decrease of mean annual precipitation of 14.5% from 1531 mm/year to 1310 mm/year. Moreover, the monthly averages of LP OrbMax show a trend of increasing seasonality, with increased precipitation in summer during the LP OrbMax run and decreased precipitation in winter, the exception being July, which shows a drop in the mean total from 184 mm in the LP run to 86 mm in the LP OrbMax run.

The PETM OrbMax run in the EMA showed a net increase in precipitation of 24.7% to 1910 mm/year, significantly lower than the PETM run. Additionally, the exceedance frequency exhibits an overall decrease in the intensity of precipitation, trailed only by the LP OrbMax run. There were marginal increases in the intensity of winter precipitation evidenced by the 3rd quartile, and variable increases or decreases in summer precipitation compared to the LP run.

Runoff in the EMA region demonstrates even greater shifts, with the PETM having the highest rates at 1230 mm/year, an increase of 179% over the 439 mm/year from the LP run. Similarly, the OrbMax configuration resulted in a decrease in total runoff, with 346 mm/year in the LP OrbMax run and 802 mm/year in the PETM OrbMax run.

4. Discussion

In terms of a hydrologic regime shift, the observed changes in the

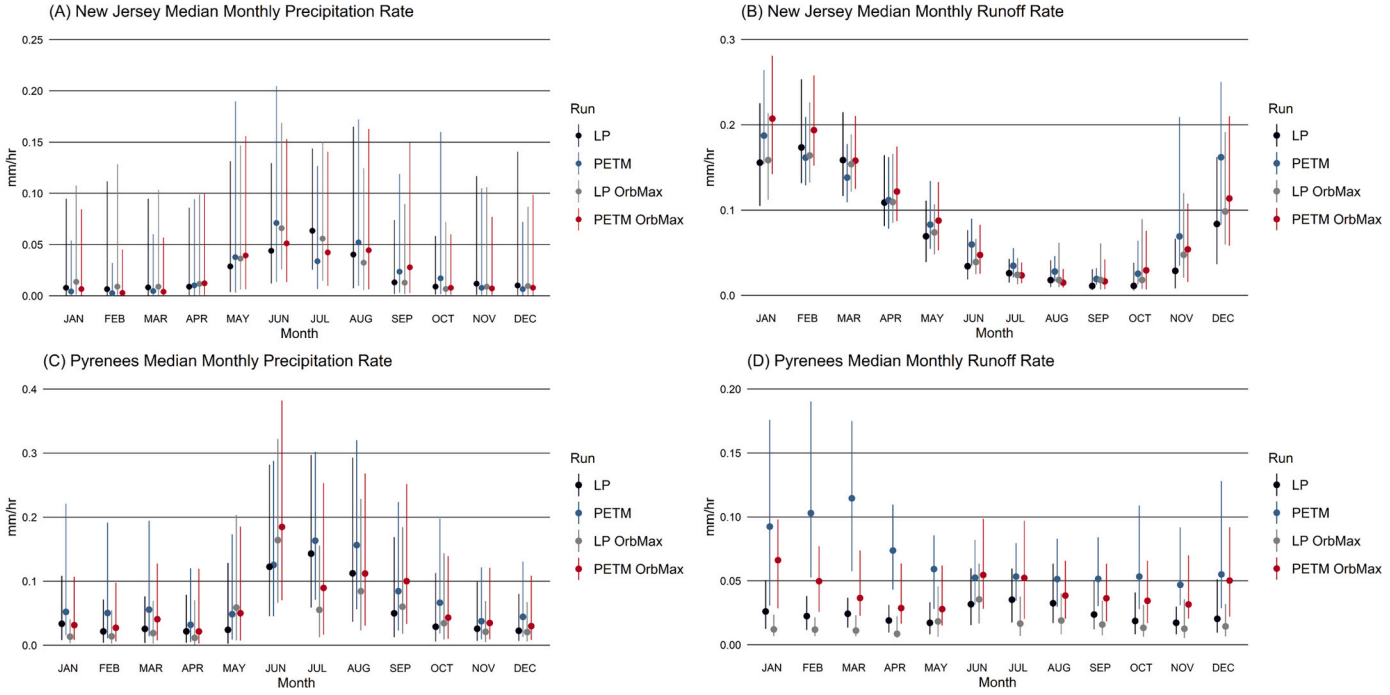

Fig. 2. Comparative modeled median precipitation (A, C) and runoff (B, D) rates in the Mid-Atlantic region (A, B) and Northern Spain (C, D) for late Paleocene and PETM CO_2 levels with and without maximizing insolation in the northern hemisphere during boreal summer. Error bars represent 1st and 3rd quartile precipitation rates. For all model runs, $n = 21{,}900$. Note increased seasonality of extreme precipitation in New Jersey during the PETM evidenced by increase in 3rd quartile in summer and decrease in winter. OrbMax runs show similar trends to their neutral orbit counterparts. For Northern Spain, note increase in intensity of winter precipitation resulting from increased CO_2 levels, but a reduction in intensity (and runoff) in the OrbMax configuration.

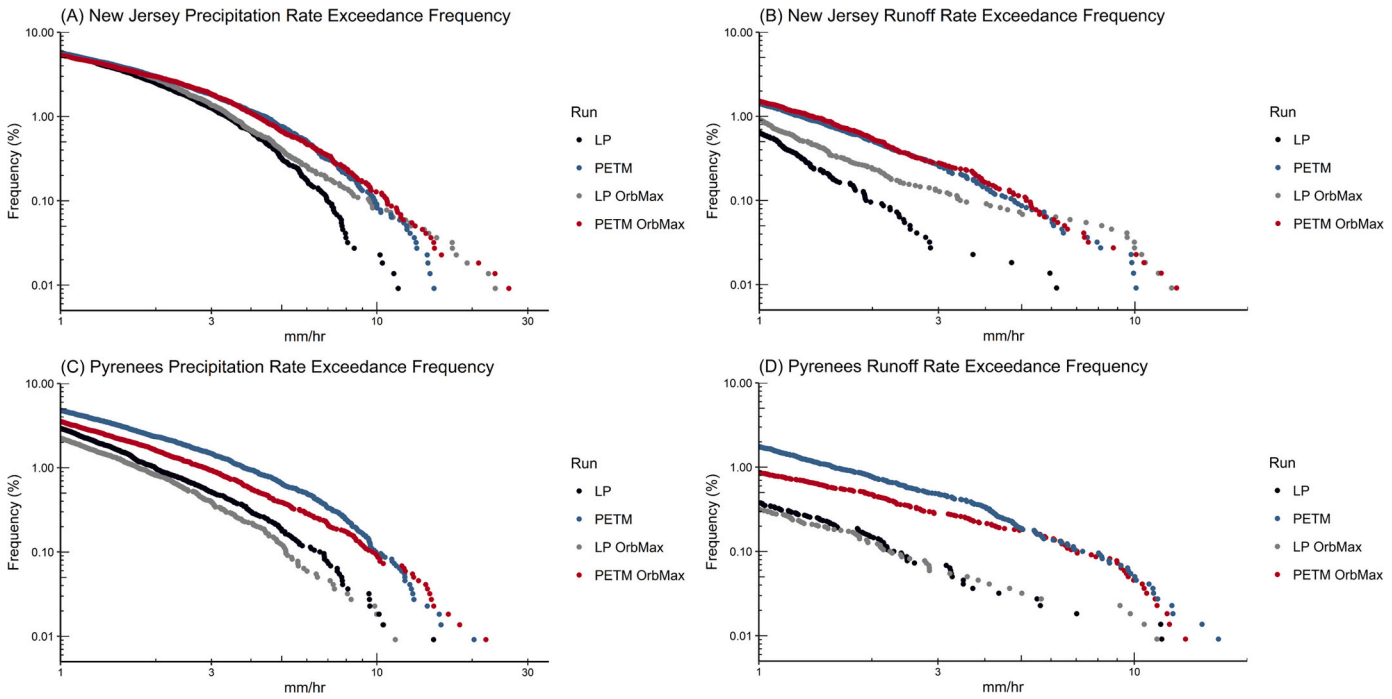

Fig. 3. Modeled exceedance frequency of precipitation (A, C) and runoff (B, D) events at late Paleocene and PETM CO_2 levels with and without maximizing solar insolation over the Northern hemisphere for the Mid-Atlantic (A, B) and Northern Spain (C, D). For all model runs, n = 21,900. For precipitation in New Jersey, note the increase in frequency and intensity of storm events in both CO_2 and orbitally forced runs. For precipitation in the Pyrenees, note increases related to CO_2 forcing, and decreases related to orbital forcing.

character of sedimentation during the PETM at the two locations considered here could be explained by the following: a change in seasonality with enhanced wet-dry cycles leading to denudation of the landscape from the dry season and the erosion of newly barren soil during the wet season (Schmitz and Pujalte 2007; Molnar et al., 2001), increasing the frequency and intensity of storm events (Molnar et al., 2001; Eden and Page 1998; Rossi et al. 2016) or by simply increasing the overall precipitation (MAP) (Langbein and Schumm 1958). These impacts are by no means exclusive from one another and may work in conjunction. For example, Anderson (1954) found levels of sediment discharge to be correlated with both fluvial discharge and the "peakedness" of the fluvial discharge, i.e. the variation between periods of low flow and periods of high flow. This relationship is somewhat complicated as these increases in precipitation driving erosion are counterbalanced by increased vegetation cover stabilizing soils, i.e. going from an arid climate to one with moderate rainfall can increase sedimentation rates, but further increases can stabilize the landscape through increased vegetation (Langbein and Schumm 1958; Nearing et al. 2005).

We first consider the simulated changes in MAP of the two mid-Atlantic coasts in response to GH forcing under neutral and maximum boreal summer insolation orbits. Both studied locations experience increases in overall MAP in response to PETM greenhouse forcing. These increases are damped slightly under the OrbMax configuration in the WMA, and more significantly in the EMA. Overall, the changes in MAP (<15%) taken on their own are inadequate to explain the observations of increased sedimentation rates in the WMA regardless of orbital configuration. These changes are greater in the EMA (>50%), however, this increase is highly seasonal, which may have influenced erosion rates (Anderson 1954; Molnar et al., 2001) (Fig. 2). In both instances, the late Paleocene background precipitation rate of 2273 mm/yr in the WMA and 1531 mm/yr in the EMA are beyond the 355 mm/yr suggested as the upper limit by Langbein and Schumm (1958) in which increases in MAP would influence sediment yields.

We next consider the intra-annual extremes of precipitation. Previous studies have found this to have a significant impact on erosion rates, more so than changes in rainfall amount alone (Nearing et al. 2005). The simulated increase in greenhouse gas forcing does significantly increase the frequency and intensity of storm events on both North Atlantic coasts as evidenced by the changes in the exceedance frequency (Fig. 3). However, the intensity of extreme precipitation varies at each location depending on orbit. The CO_2 forcing increases the frequency and intensity of extreme precipitation events on both coasts, but maximizing solar insolation during boreal summer resulted in differing signals. The EMA experienced a drop in frequency in the moderate events (<5 mm/h) in response to the OrbMax forcing, while the extreme events (>5 mm/h) were comparable to, and often exceeded the neutral orbit runs in both frequency and intensity. The WMA frequency of extreme precipitation was largely the same between the neutral orbit and OrbMax runs for moderate events regardless of CO_2 forcing, but the OrbMax runs experienced an increase in the frequency of extreme events, particularly for the LP CO_2 levels (Fig. 3).

The drop in moderate scale events in the EMA under the OrbMax configuration appears to be due at least in part to the seasonality of extreme precipitation events. While extreme precipitation in the Mid-Atlantic occurs primarily during boreal summer months, the greatest change to extreme precipitation in the Pyrenees occurred during boreal winter months (Fig. 2). This damped response under OrbMax can be attributed to the reduction in energy in the northern hemisphere during winter months as insolation is concentrated in summer months (i.e., perihelion). In this regard, future characterization of extreme precipitation events during the PETM should focus on extending the duration of the model runs to analyze shifts in more infrequent, stronger storms, e.g. 100-year storms, as well as testing the effects of maximizing insolation during boreal winter, i.e. aphelion.

In the WMA, both the PETM run and the PETM OrbMax run demonstrate significantly increased precipitation during the summer months alongside slightly drier conditions in winter months compared to the neutral orbit late Paleocene run. This has the potential to shift the hydrodynamics of regional catchments to a more erosive state (Schmitz

and Pujalte 2007; Molnar et al., 2001). Combined with the increased storm activity (Figs. 2, 3 and S2) and increases in mean annual runoff on 36.8% compared to LP run, this supports the observations of increases in regional sedimentation rates of 2.8 to 220-fold late Paleocene values (Stassen et al. 2012), the sudden abundance of more low-salinity tolerant dinoflagellate cysts (Sluijs and Brinkhuis 2009), and the appearance of bacterial magnetofossils associated with high discharge environments (Kopp et al. 2009).

In the EMA, the modeled changes are broadly in agreement with observations. The deposition of the Claret Conglomerate with clasts of up to 65 cm alongside a flux of kaolinite to the Basque Basin indicate a strengthening of the hydrologic cycle (Schmitz and Pujalte 2007; Schmitz et al. 2001). Estimates of streamflow in the region based on channel dimensions estimate an increase in discharge of 1.35 to 14.9-fold (Chen et al. 2018). This is consistent with the modeled predictions of an increase in mean annual runoff of 2.79-fold from the PETM run compared to the LP run. The modeled changes in precipitation can be linked to an increase in the intensity of atmospheric river related precipitation (Shields et al., 2021). Although the timing of sediment changes relative to the onset of the PETM in this region has been controversial on the basis of defining lithologic units (Pujalte and Schmitz 2014), if the interpretations of Duller et al. 2019 are correct, the observed delays ($\sim 16 \pm 7.5$ k.y.) may be related to orbital variation, as the OrbMax configuration results in a suppression of precipitation and runoff, both in the late Paleocene and the PETM (with precession, the delay would be ~10 k.y.). If these interpretations are not correct, it is possible that the reduced hydrologic activity noted in the OrbMax configuration of the model may have resulted in a period of nondeposition or was eroded by later, more intense hydrologic activity.

Delving into the model beyond the simulated changes in precipitation, the dynamical forcing seems to fit with these interpretations. Eddy kinetic energy, defined as $(\boldsymbol{u}'^2 + \boldsymbol{v}'^2)/\mathbf{2}$, wherein $\boldsymbol{u}'$ is the zonal component of the difference between the instantaneous and average wind velocity ($\boldsymbol{u}' = \boldsymbol{u} - \overline{\boldsymbol{u}}$), and $\boldsymbol{v}'$ is the meridional component, can be used as a means of analyzing changes in storm tracks (O'Gorman 2010). For boreal winter, there is a reduction in eddy kinetic energy in the Mid-Atlantic region in response to both higher CO_2 and NH insolation (Fig. S2). These observations are in line with the reduction in precipitation. The Iberian Peninsula experiences drops in eddy kinetic energy in the OrbMax runs, but increases in response to CO_2, again in line with precipitation changes.

Changes to eddy kinetic energy in boreal summer are much more complicated, with very different signals between the 250 mbar and 700 mbar pressure levels, indicating much of the precipitation for both locations during this season is not necessarily linked to large scale jets or the jet-driven storm tracks. Focusing on the Mid-Atlantic, during this season, there is a significant increase in convective precipitation during the PETM runs compared to the LP runs, while non-convective, large-scale precipitation remains relatively constant, indicating these changes are likely due to locally generated thunderstorms (not shown). However, holding CO_2 constant and maximizing summer insolation via orbit results in greater changes to large-scale precipitation than convective, suggesting precipitation is related to surface lows or frontal boundaries, but are are just surface disturbances clearly not connected to the steering flow.

In Northern Spain, the GHG forcing results in increases in both convective and large-scale precipitation particularly during winter months, the most significant being increases in large scale storm tracks, likely driven by an increase in atmospheric river activity, which are most active in the winter months in this region. In the OrbMax configuration, however, both are reduced.

5. Conclusions

Model predictions demonstrate both the Mid-Atlantic and Northern Spain experienced significant changes in hydroclimate as a result of higher CO_2 during the PETM. The most prominent changes are increases in the frequency and intensity of precipitation events and the seasonal timing of these events, which are likely the driver of the observed changes in sedimentation. These modeled changes are broadly in agreement with observations in each region. However, compounding the effects of CO_2 forcing with changes in orbit results in divergent signals, with the Mid-Atlantic region staying largely in line with the changes from CO_2 alone, and the Pyrenees seeing a suppression of the effects of CO_2 forcing. These varying responses may contribute to the observed variation in the timing of hydrologic changes relative to the carbon isotope excursion on either side of the Atlantic. On balance, the agreement between models and observations of the PETM increases confidence in general theory of intensification of the hydrologic cycle in response to significant increases in greenhouse gas levels in Earth's past and in the not so distant future. This includes the increased frequency of extreme precipitation events.

Acknowledgments and data

Mathew Rothstein and Mark Snyder contributed to model construct. Funding for this project was provided by a Heising-Simons Foundation Grant to JTK, an NSF grant (OCE-1415958) to JCZ and the Ida Benson Lynn Foundation. Modeling conducted by Jeff Kiehl and Christine Shields. Data analysis and interpretation performed by William Rush. James Zachos and Jeff Kiehl conceived and supervised the project. WR wrote the manuscript with contributions from all co-authors.

Model output was generated using the CAM5.3 FV (finite volume) dynamical core high-resolution (0.25 degree version) model run for 20 years (Neale et al. 2010; Park et al. 2014), with CLM4.0 for the land component (Lawrence et al. 2011), and MEGAN for the aerosol emissions (Guenther et al. 2012). Sea surface temperatures for CAM were fixed using CESM1.2.2, which was run for 1800 years and fully coupled for boundary conditions, and is publicly available at http://www2.cesm.ucar.edu/models/cesm1.2/. Boundary data including topography, bathymetry, and land use were obtained from the DeepMIP repository (Lunt et al. 2017). Total model output for these model runs is stored on the NCAR computing cluster, and may be accessed by contacting Christine Shields (shields@ucar.edu). Model output used in generation of figures is available for download through Dryad, an open-source online data repository at https://datadryad.org/stash/dataset/doi:10.7291/D1FQ18.

Declaration of Competing Interest

The authors declare that they have no known competing financial interests or personal relationships that could have appeared to influence the work reported in this paper.

The authors declare the following financial interests/personal relationships which may be considered as potential competing interests.

Appendix A. Supplementary data

Supplementary data to this article can be found online at https://doi.org/10.1016/j.palaeo.2021.110289.

References

Anderson, H.W., 1954. Suspended sediment discharge as related to streamflow, topography, soil, and land use. EOS Trans. Am. Geophys. Union 35 (2), 268–281. https://doi.org/10.1029/TR035i002p00268.

Arakawa, A., 2004. The cumulus parameterization problem: past, present, and future. J. Clim. 17, 2493–2525. https://doi.org/10.1175/1520-0442(2004)017<2493:RATCPP>2.0.CO;2.

Carmichael, M.J., Pancost, R.D., Lunt, D.J., 2018. Changes in the occurrence of extreme precipitation events at the Paleocene–Eocene thermal maximum. Earth Planet. Sci. Lett. 501, 24–36. https://doi.org/10.1016/j.epsl.2018.08.005.

Chen, Z., Ding, Z., Yang, S., Zhang, C., Wang, X., 2016. Increased precipitation and weathering across the paleocene-eocene thermal maximum in Central China. Geochem. Geophys. Geosyst. 17 (6), 2286–2297. https://doi.org/10.1002/2016GC006333.

Chen, C., Guerit, L., Foreman, B.Z., Hassenruck-Gudipati, H.J., Adatte, T., Honegger, L., Perret, M., Sluijs, A., Castelltort, S., 2018. Estimating regional flood discharge during palaeocene-eocene global warming. Sci. Rep. 8 (1), 1–8. https://doi.org/10.1038/s41598-018-31076-3.

Christensen, H.M., 2020. Constraining stochastic parametrisation schemes using high-resolution simulations. Q. J. R. Meteorol. Soc. 146, 938–962. https://doi.org/10.1002/qj.3717.

Duller, R.A., Armitage, J.J., Manners, H.R., Grimes, S., Jones, T.D., 2019. Delayed sedimentary response to abrupt climate change at the Paleocene-Eocene boundary, northern Spain. Geology 47 (2), 159–162. https://doi.org/10.1130/G45631.1.

Dunkley Jones, T., Manners, H.R., Hoggett, M., Kirtland Turner, S., Westerhold, T., Leng, M.J., Pancost, R.D., Ridgwell, A., Alegret, L., Duller, R., Grimes, S.T., 2018. Dynamics of sediment flux to a bathyal continental margin section through the Paleocene–Eocene thermal maximum. Clim. Past 14 (7), 1035–1049. https://doi.org/10.5194/cp-14-1035-2018.

Eden, D.N., Page, M.J., 1998. Palaeoclimatic implications of a storm erosion record from late Holocene lake sediments, North Island, New Zealand. Palaeogeogr. Palaeoclimatol. Palaeoecol. 139 (1–2), 37–58. https://doi.org/10.1016/S0031-0182(97)00136-3.

Gibson, T.G., Bybell, L.M., Mason, D.B., 2000. Stratigraphic and climatic implications of clay mineral changes around the Paleocene/Eocene boundary of the northeastern US margin. Sediment. Geol. 134 (1–2), 65–92. https://doi.org/10.1016/S0037-0738(00)00014-2.

Guenther, A.B., Jiang, X., Heald, Colette L., Sakulyanontvittaya, T., Duhl, T., Emmons, L. K., Wang, X., 2012. The model of emissions of gases and aerosols from nature version 2.1 (MEGAN2. 1): an extended and updated framework for modeling biogenic emissions. Geosci. Model Dev. 5, 1471–1492. https://doi.org/10.5194/gmd-5-1471-2012.

Gutjahr, M., Ridgwell, A., Sexton, P.F., Anagnostou, E., Pearson, P.N., Pälike, H., Norris, R.D., Thomas, E., Foster, G.L., 2017. Very large release of mostly volcanic carbon during the Palaeocene–Eocene thermal maximum. Nature 548 (7669), 573–577. https://doi.org/10.1038/nature23646.

Handley, L., O'Halloran, A., Pearson, P.N., Hawkins, E., Nicholas, C.J., Schouten, S., McMillan, I.K., Pancost, R.D., 2012. Changes in the hydrological cycle in tropical East Africa during the Paleocene–Eocene thermal maximum. Palaeogeogr. Palaeoclimatol. Palaeoecol. 329, 10–21. https://doi.org/10.1016/j.palaeo.2012.02.002.

Held, I.M., Soden, B.J., 2006. Robust responses of the hydrological cycle to global warming. J. Clim. 19 (21), 5686–5699. https://doi.org/10.1175/JCLI3990.1.

Jakob, C., 2010. Accelerating progress in global atmospheric model development through improved parameterizations: challenges, opportunities, and strategies. Bull. Am. Meteorol. Soc. 91, 869–875. https://doi.org/10.1175/2009BAMS2898.1.

John, C.M., Bohaty, S.M., Zachos, J.C., Sluijs, A., Gibbs, S., Brinkhuis, H., Bralower, T.J., 2008. North American continental margin records of the Paleocene-Eocene thermal maximum: Implications for global carbon and hydrological cycling. Paleoceanography 23 (2). https://doi.org/10.1029/2007PA001465.

John, C.M., Banerjee, N.R., Longstaffe, F.J., Sica, C., Law, K.R., Zachos, J.C., 2012. Clay assemblage and oxygen isotopic constraints on the weathering response to the Paleocene-Eocene thermal maximum, east coast of North America. Geology 40 (7), 591–594. https://doi.org/10.1130/G32785.1.

Kemp, S.J., Ellis, M.A., Mounteney, I., Kender, S., 2016. Palaeoclimatic implications of high-resolution clay mineral assemblages preceding and across the onset of the Palaeocene–Eocene thermal maximum, North Sea Basin. Clay Miner. 51 (5), 793–813. https://doi.org/10.1180/claymin.2016.051.5.08.

Kiehl, J.T., Shields, C.A., Snyder, M.A., Zachos, J.C., Rothstein, M., 2018. Greenhouse- and orbital-forced climate extremes during the early Eocene. Philos. Trans. R. Soc. A Math. Phys. Eng. Sci. 376 (2130) https://doi.org/10.1098/rsta.2017.0085, 20170085.

Kiehl J.T.; Zarzycki C.M.; Shields C.A.; Rothstein M.V., in Review. Simulated changes to tropical cyclones across the Paleocene Eocene thermal Maximum (PETM) Boundary. Palaeogeogr. Palaeoclimatol. Palaeoecol.

Kopp, R.E., Schumann, D., Raub, T.D., Powars, D.S., Godfrey, L.V., Swanson-Hysell, N.L., Maloof, A.C., Vali, H., 2009. An Appalachian Amazon? Magnetofossil evidence for the development of a tropical river-like system in the mid-Atlantic United States during the Paleocene-Eocene thermal maximum. Paleoceanogr. Paleoclimatol. 24 (4) https://doi.org/10.1029/2009PA001783.

Laing, A., Evans, J.L., 2011. Introduction to Tropical Meteorology (Educational material from The COMET Program).

Langbein, W.B., Schumm, S.A., 1958. Yield of sediment in relation to mean annual precipitation. EOS Trans. Am. Geophys. Union 39 (6), 1076–1084. https://doi.org/10.1029/TR039i006p01076.

Lawrence, D.M., Oleson, K.W., Flanner, M.G., Thornton, P.E., Swenson, S.C., Lawrence, P.J., Zeng, X., Yang, Z.L., Levis, S., Sakaguchi, K., Bonan, G.B., 2011. Parameterization improvements and functional and structural advances in version 4 of the community land model. J. Adv. Model. Earth Syst. 3 (1) https://doi.org/10.1029/2011MS00045.

Lippert, P.C., Zachos, J.C., 2007. A biogenic origin for anomalous fine-grained magnetic material at the Paleocene-Eocene boundary at Wilson Lake, New Jersey. Paleoceanography 22 (4). https://doi.org/10.1029/2007PA001471.

Littler, K., Röhl, U., Westerhold, T., Zachos, J.C., 2014. A high-resolution benthic stable-isotope record for the South Atlantic: implications for orbital-scale changes in Late Paleocene–Early Eocene climate and carbon cycling. Earth Planet. Sci. Lett. 401, 18–30. https://doi.org/10.1016/j.epsl.2014.05.054.

Lunt, D.J., Huber, M., Anagnostou, E., Baatsen, M.L.J., Caballero, R., DeConto, R., Dijkstra, H.A., Donnadieu, Y., Evans, D., Feng, R., Foster, G.L., 2017. The DeepMIP contribution to PMIP4: experimental design for model simulations of the EECO, PETM, and pre-PETM (version 1.0). Geosci. Model Dev. 10, 889–901. https://doi.org/10.5194/gmd-10-889-2017.

Lyons, S.L., Baczynski, A.A., Babila, T.L., Bralower, T.J., Hajek, E.A., Kump, L.R., Polites, E.G., Self-Trail, J.M., Trampush, S.M., Vornlocher, J.R., Zachos, J.C., 2019. Palaeocene–Eocene thermal maximum prolonged by fossil carbon oxidation. Nat. Geosci. 12 (1), 54–60. https://doi.org/10.1038/s41561-018-0277-3.

McFarlane, N., 2011. Parameterizations: representing key processes in climate models without resolving them. Wiley Interdiscip. Rev. Clim. Chang. 2, 482–497. https://doi.org/10.1002/wcc.122.

McInerney, F.A., Wing, S.L., 2011. The Paleocene-Eocene thermal maximum: a perturbation of carbon cycle, climate, and biosphere with implications for the future. Annu. Rev. Earth Planet. Sci. 39, 489–516. https://doi.org/10.1146/annurev-earth-040610-133431.

Molnar, P., 2001. Climate change, flooding in arid environments, and erosion rates. Geology 29 (12), 1071–1074. https://doi.org/10.1130/0091-7613(2001)029<1071:CCFIAE>2.0.CO;2.

Neale, R.B., Chen, C.C., Gettelman, A., Lauritzen, P.H., Park, S., Williamson, D.L., Conley, A.J., Garcia, R., Kinnison, D., Lamarque, J.F., Marsh, D., 2010. Description of the NCAR community atmosphere model (CAM5.0). In: NCAR Technical Reports, NCAR/TN-486+STR, pp. 1–12.

Nearing, M.A., Jetten, V., Baffaut, C., Cerdan, O., Couturier, A., Hernandez, M., Le Bissonnais, Y., Nichols, M.H., Nunes, J.P., Renschler, C.S., Souchère, V., 2005. Modeling response of soil erosion and runoff to changes in precipitation and cover. Catena 61 (2–3), 131–154.

O'Gorman, P.A., 2010. Understanding the varied response of the extratropical storm tracks to climate change. Proc. Natl. Acad. Sci. 107 (45), 19176–19180. https://doi.org/10.1073/pnas.1011547107.

Park, S., Bretherton, C.S., Rasch, P.J., 2014. Integrating cloud processes in the community atmosphere model, Version 5. J. Clim. 27, 6821–6856. https://doi.org/10.1175/JCLI-D-14-00087.1.

Pfahl, S., O'Gorman, P.A., Fischer, E.M., 2017. Understanding the regional pattern of projected future changes in extreme precipitation. Nat. Clim. Chang. 7 (6), 423–427. https://doi.org/10.1038/nclimate3287.

Pujalte, V., Schmitz, B., 2014. Comment on" magnitude and profile of organic carbon isotope records from the Paleocene-Eocene thermal maximum: evidence from northern Spain" by Manners et al.[Earth Planet. Sci. Lett. 376 (2013) 220-230]. Earth Planet. Sci. Lett. 395, 291–293. https://doi.org/10.1016/j.epsl.2014.03.054.

Pujalte, V., Baceta, J.I., Schmitz, B., 2015. A massive input of coarse-grained siliciclastics in the Pyrenean Basin during the PETM: the missing ingredient in a coeval abrupt change in hydrological regime. Clim. Past 11 (12). https://doi.org/10.5194/cp-11-1653-2015.

Ralph, F.M., 2019. Atmospheric Rivers. Springer Nature.

Robert, C., Kennett, J.P., 1994. Antarctic subtropical humid episode at the Paleocene-Eocene boundary: clay-mineral evidence. Geology 22 (3), 211–214. https://doi.org/10.1130/0091-7613(1994)022<0211:ASHEAT>2.3.CO;2.

Rossi, M.W., Whipple, K.X., Vivoni, E.R., 2016. Precipitation and evapotranspiration controls on daily runoff variability in the contiguous United States and Puerto Rico. J. Geophys. Res. Earth Surf. 121 (1), 128–145. https://doi.org/10.1002/2015JF003446.

Schmitz, B., Pujalte, V., 2007. Abrupt increase in seasonal extreme precipitation at the Paleocene-Eocene boundary. Geology 35 (3), 215–218. https://doi.org/10.1130/G23261A.1.

Schmitz, B., Pujalte, V., Nunez-Betelu, K., 2001. Climate and sea-level perturbations during the incipient Eocene thermal maximum: evidence from siliciclastic units in the Basque Basin (Ermua, Zumaia and Trabakua Pass), northern Spain. Palaeogeogr. Palaeoclimatol. Palaeoecol. 165 (3–4), 299–320. https://doi.org/10.1016/S0031-0182(00)00167-X.

Self-Trail, J.M., Robinson, M.M., Bralower, T.J., Sessa, J.A., Hajek, E.A., Kump, L.R., Trampush, S.M., Willard, D.A., Edwards, L.E., Powars, D.S., Wandless, G.A., 2017. Shallow marine response to global climate change during the Paleocene-Eocene thermal maximum, Salisbury Embayment, USA. Paleoceanography 32 (7), 710–728. https://doi.org/10.1002/2017PA003096.

Shields, C.A., Kiehl, J.T., Rush, W.D., Rothstein, M., Snyder, M.A., 2021. Atmospheric rivers in high-resolution simulations of the Paleocene Eocene thermal Maximum (PETM). Palaeogeogr. Palaeoclimatol. Palaeoecol. 567C https://doi.org/10.1016/j.palaeo.2021.110293.

Sluijs, A., Brinkhuis, H., 2009. A dynamic climate and ecosystem state during the Paleocene-Eocene thermal Maximum: inferences from dinoflagellate cyst assemblages on the New Jersey Shelf. Biogeosciences 6 (8), 1755–1781. https://doi.org/10.5194/bg-6-1755-2009.

Stassen, P., Thomas, E., Speijer, R.P., 2012. Integrated stratigraphy of the Paleocene-Eocene thermal maximum in the New Jersey Coastal Plain: toward understanding the effects of global warming in a shelf environment. Paleoceanography 27 (4). https://doi.org/10.1029/2012PA002323.

Zeebe, R.E., Lourens, L.J., 2019. Solar System chaos and the Paleocene–Eocene boundary age constrained by geology and astronomy. Science 365 (6456), 926–929. https://doi.org/10.1126/science.aax0612.

Zeebe, R.E., Zachos, J.C., 2013. Long-term legacy of massive carbon input to the Earth system: Anthropocene versus Eocene. Philos. Trans. R. Soc. A Math. Phys. Eng. Sci. 371 https://doi.org/10.1098/rsta.2012.0006, 20120006.

Zeebe, R.E., Zachos, J.C., Dickens, G.R., 2009. Carbon dioxide forcing alone insufficient to explain Palaeocene–Eocene thermal maximum warming. Nat. Geosci. 2 (8), 576–580. https://doi.org/10.1038/ngeo578.